Rapid Communications | Editors' Suggestion

Disorder-induced half-integer quantized conductance plateau in quantum anomalous Hall insulator-superconductor structures

Yingyi Huang,[1,2] F. Setiawan,[1] and Jay D. Sau[1]

[1]*Condensed Matter Theory Center and Joint Quantum Institute, Department of Physics, University of Maryland, College Park, Maryland 20742, USA*

[2]*State Key Laboratory of Optoelectronic Materials and Technologies, School of Physics, Sun Yat-sen University, Guangzhou 510275, China*

(Received 15 September 2017; published 9 March 2018)

A weak superconducting proximity effect in the vicinity of the topological transition of a quantum anomalous Hall system has been proposed as a venue to realize a topological superconductor (TSC) with chiral Majorana edge modes (CMEMs). A recent experiment [Science **357**, 294 (2017)] claimed to have observed such CMEMs in the form of a half-integer quantized conductance plateau in the two-terminal transport measurement of a quantum anomalous Hall-superconductor junction. Although the presence of a superconducting proximity effect generically splits the quantum Hall transition into two phase transitions with a gapped TSC in between, in this Rapid Communication we propose that a nearly flat conductance plateau, similar to that expected from CMEMs, can also arise from the percolation of quantum Hall edges well before the onset of the TSC or at temperatures much above the TSC gap. Our Rapid Communication, therefore, suggests that, in order to confirm the TSC, it is necessary to supplement the observation of the half-quantized conductance plateau with a hard superconducting gap (which is unlikely for a disordered system) from the conductance measurements or the heat transport measurement of the transport gap. Alternatively, the half-quantized thermal conductance would also serve as a smoking-gun signature of the TSC.

DOI: 10.1103/PhysRevB.97.100501

Recent years have seen a burgeoning interest in realizing topological superconductors (TSCs) which host zero-energy Majorana modes. These Majorana zero modes hold potential applications for a fault-tolerant topological quantum computation [1] owing to their non-Abelian braiding statistics [2,3]. They can be found in the vortex core of a two-dimensional (2D) chiral TSC with an odd integer Chern number. Recent theoretical studies [4–6] proposed to realize this chiral TSC using a quantum anomalous Hall insulator (QAHI) in proximity to an s-wave superconductor (SC).

The quantum anomalous Hall (QAH) state is a quantum Hall (QH) state without an external magnetic field which can be realized in a 2D thin film of a magnetic topological insulator (TI) with ferromagnetic ordering [7–11]. For the regime where the ferromagnetic-induced exchange field strength $|\lambda|$ is greater than the hybridization gap $|m_0|$ induced by the coupling between the top and the bottom surfaces, the system has a Chern number of $\mathcal{C} = \lambda/|\lambda|$ and in the opposite limit where $|\lambda| < |m_0|$, $\mathcal{C} = 0$ [6,12]. By changing the applied magnetic field over a relatively small range, a topological phase transition can be induced between the QAHI with $\mathcal{C} = 1$ and the trivial insulator state with $\mathcal{C} = 0$ [13]. When the QAH is proximitized by an s-wave SC, the $\mathcal{C} = 1$ and $\mathcal{C} = 0$ phases are driven into $\mathcal{N} = 2$ and $\mathcal{N} = 0$ phases [4], respectively, where $\mathcal{N}$ denotes the number of chiral Majorana edge mode (CMEM). At the transition between these two phases, there exists an $\mathcal{N} = 1$ gapped TSC [4,5]. Since a single CMEM carries one-half of the incoming charges, it manifests as a half-integer quantized $e^2/2h$ plateau in the conductance between two normal leads and an integer quantized e^2/h peak in the conductance between a normal lead and the SC measured at the coercive field [5,6]. A recent experiment [14] observed these two transport signatures in a doped magnetic QAHI thin film proximitized by an s-wave SC. Although these transport signatures are consistent with the existence of an $\mathcal{N} = 1$ TSC with a single CMEM in a clean system, the disorder in the experimental system might significantly reduce the topological gap and phase space of the $\mathcal{N} = 1$ TSC.

In this Rapid Communication, we show that the two proposed transport signatures for the $\mathcal{N} = 1$ phase can generically occur in a disordered QAHI-SC-QAHI junction even in phases where the CMEM is absent, such as in the $\mathcal{C} = 1$ ($\mathcal{N} = 2$) phase or in the $\mathcal{N} = 1$ TSC but at temperatures above the gap. We consider the disordered QAH system to be inhomogeneous with smoothly varying magnetization [15] which leads to a network of domain walls between phases with different Chern numbers. Such domain walls have been invoked in Ref. [16] to understand the Hall conductance in this system. Here, we consider the disorder strength to be stronger than the superconducting pairing potential such that there are no $\mathcal{N} = 1$ domains in the system.

Figure 1 shows the evolution of the domain-wall structure of the phases in the QAH system as the magnetic field is varied. In the limit of strong magnetic field, the system is in a single-domain $\mathcal{C} = 1$ phase [as shown in Fig. 1(a)] with a large average magnetization. In this regime, the edge states are perfectly transmitted across the junction. During the magnetization reversal, the proportion p of the $\mathcal{C} = 0$ domain (domain with small average magnetization) increases [Fig. 1(b)]. Since the chiral edge states live at the boundary between the $\mathcal{C} = 0$ and

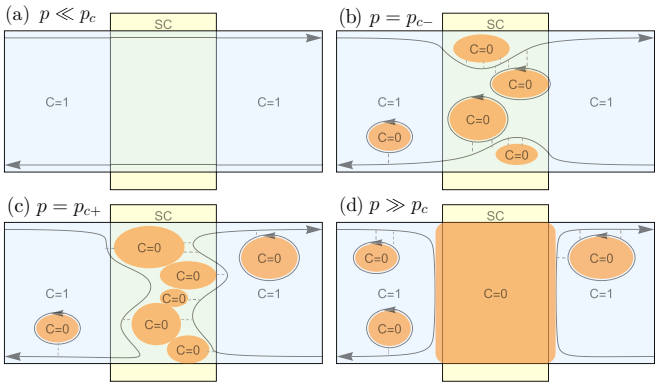

FIG. 1. Schematics of the magnetic-field-induced percolation in a disordered QAHI-SC-QAHI junction. The middle QAHI region is proximitized by an s-wave SC (the yellow rectangle). Four different percolation stages of trivial insulator phases (the orange region) with $\mathcal{C} = 0$ (corresponding to $\mathcal{N} = 0$) and QAHI phases (the light-blue region) with $\mathcal{C} = 1$ (corresponding to $\mathcal{N} = 2$). We consider a strongly disordered system where $\mathcal{N} = 1$ domains do not form. The four stages are characterized by p, the proportion of the $\mathcal{C} = 0$ phase, which changes with the magnetic field. (a) In the strong magnetic-field regime where p is far below the percolation threshold ($p \ll p_c$), the system is in the $\mathcal{C} = 1$ phase. The edge states (shown by the arrowed lines) are perfectly transmitted across the junction. (b) During the magnetization reversal, the $\mathcal{C} = 0$ phase domains grow. The edge states wind around the domains in the SC region and leak into adjacent chiral loops (shown by the dashed lines). (c) When p is slightly above the percolation threshold ($p = p_{c+}$), the domains are connected across the junction width, and the edge states can no longer be transmitted across the junction. (d) When $p \gg p_c$, the edge states are normally reflected by the $\mathcal{C} = 0$ phase outside the SC region.

the $\mathcal{C} = 1$ domains, the edge state has to wind around the $\mathcal{C} = 0$ domains which increases the electron trajectory length L and hence the number of Andreev scatterings in the SC region. As p approaches the percolation threshold p_c (where the $\mathcal{C} = 0$ domains become connected into a cluster spanning across the junction width), $L \to \infty$. In addition, quasiparticles on the chiral edge can leak by quantum tunneling into adjacent chiral loops associated with the domains as shown in Fig. 1. These chiral loops can be assumed to be in equilibrium. As a result, at $p \approx p_c$, as we will show, the leakage of quasiparticles leads to eventual absorption of the initial quasiparticle for large lengths L, giving rise to a nearly flat $e^2/2h$ two-terminal conductance plateau. As p increases above p_c, the edge states can no longer be transmitted across the junction. For $p \gg p_c$, the electrons undergo perfect normal reflections outside the SC region by the $\mathcal{C} = 0$ domain as shown in Fig. 1(d).

We describe the low-energy edge modes of the QAHI-SC structure by a one-dimensional Hamiltonian,

$$H = \frac{1}{2}\int dx\, \mathcal{C}^\dagger(x)\mathcal{H}_{\mathrm{BdG}}(x)\mathcal{C}(x), \tag{1}$$

where

$$\mathcal{H}_{\mathrm{BdG}}(x) = -iv\tau_0\partial_x - \mu(x)\tau_z + \tfrac{1}{2}\{-i\partial_x, \Delta(x)\tau_x\} \tag{2}$$

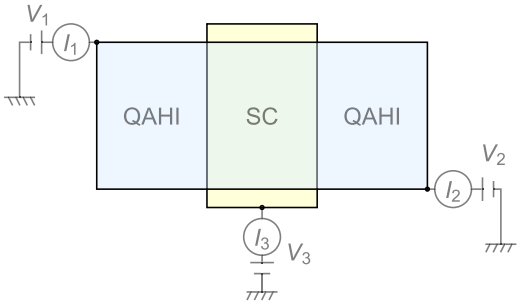

FIG. 2. Schematic of the setup used to measure the conductance in a QAHI-SC-QAHI junction. To measure G_{12}, we consider the SC to be floating (i.e., $I_3 = 0$) and the voltages V_1 and V_2 to be applied to leads 1 and 2, respectively. For the case where G_{13} is measured, the SC is grounded (i.e., $I_3 \neq 0$), lead 2 is removed, and the voltages V_1 and V_3 are applied to lead 1 and the SC, respectively.

is the Bogoliubov–de Gennes (BdG) Hamiltonian and $\mathcal{C}(x) = [c(x), c^\dagger(x)]^T$ is the Nambu spinor with $c(x)$ and $c^\dagger(x)$ being the electron annihilation and creation operators, respectively. Here, v is the edge mode velocity, μ is the chemical potential, Δ is the effective p-wave pairing potential of the proximity-induced superconductivity, and $\tau_{x,y,z}$ are the Pauli matrices in the particle-hole space. For the QAHI region, we set $\Delta = 0$, whereas for the SC region, we set $\mu(x)$ and $\Delta(x)$ to be spatially varying along the electron trajectory length L. For simplicity, we work in the units where the Planck constant $\hbar$, the Boltzmann constant k_B, and edge velocity v are all set to 1. We note that the term ∂_x in the Hamiltonian comes with the anticommutation relation $\{,\}$ to ensure the Hermiticity of the Hamiltonian. The p-wave pairing amplitude $\Delta(x)$ is induced from the proximity effect of an s-wave SC with a pairing potential $\Delta_s(x)$. This cannot occur in a strictly spin-polarized edge state. However, since the QAH system arises from a TI, which is a strongly spin-orbit-coupled system, we expect the spin polarization of the chiral edge state to vary with momentum (similar to the spin texture in a TI [17] on a scale of the spin-orbit length k_{so}^{-1} where k_{so} is related to the exchange field λ by $k_{\mathrm{so}} \sim \lambda/v$). Within this model, $\Delta(x) \sim v\Delta_s(x)/\lambda$ (see the Supplemental Material [18] for the derivation).

The conductance of the three-terminal junction shown in Fig. 2 where terminal 3 is connected to the SC can be computed from Bogoliubov quasiparticle transmission and reflection probabilities using a generalized Landauer-Büttiker formalism [19–21]. Using this formalism the currents $I_{1,2}$ shown in Fig. 2 are found to be

$$I_1 = \frac{e^2}{h}[(1 - g_{11})(V_1 - V_3) - g_{12}(V_2 - V_3)], \tag{3a}$$

$$I_2 = \frac{e^2}{h}[-g_{21}(V_1 - V_3) + (1 - g_{22})(V_2 - V_3)], \tag{3b}$$

where V_1 and V_2 are the voltages of leads 1 and 2, respectively, V_3 is the voltage of the SC, and g_{ij} are effective dimensionless conductances from lead i to lead j due to the chiral edges. Experimentally, the conductance is measured using a two-terminal setup, i.e., the setup in Fig. 2 with either the current

$I_2 = 0$ (grounding) or $I_3 = 0$ (floating SC case) depending on the measured transport properties. For the case of floating SC, we obtain the conductance between leads 1 and 2 from Eq. (3) and the current conservation equation ($I_1 + I_2 = 0$) as

$$G_{12} \equiv \frac{I_1}{V_1 - V_2} = \frac{e^2}{h}\left[\frac{g_{21}g_{12} - (1-g_{11})(1-g_{22})}{g_{12}+g_{21}+g_{11}+g_{22}-2}\right]. \quad (4)$$

For the case where the SC is grounded, lead 2 is removed ($I_2 = 0$), and the conductance between lead 1 and the SC can be obtained from Eq. (3) to be

$$G_{13} \equiv \frac{I_1}{V_1 - V_3} = \frac{e^2}{h}\left[\frac{(1-g_{11})(1-g_{22}) - g_{12}g_{21}}{1-g_{22}}\right]. \quad (5)$$

To compute the parameters g_{ij} that determine the measured conductances [Eqs. (4) and (5)], we need to consider a microscopic model of the chiral edges in the vicinity of the SC. For $p < p_c$, we assume that $g_{11} = g_{22} = 0$ as the chiral edge state emanating from I_1 can only be transmitted to I_2, whereas for $p > p_c$, $g_{12} = g_{21} = 0$ as the edge states can only undergo reflection. The above condition holds in the typical case where the width of the system is larger than the correlation length at some finite distance away from the critical point such that the edge states (as shown in Fig. 1) do not couple to each other. For computational simplicity, we assume that the conductances are the same for the left- and right-incoming modes, i.e., $g_{12} = g_{21}$ and $g_{11} = g_{22}$ which is true for a symmetric junction. Our results, however, hold in general and do not qualitatively depend on this assumption.

The microscopic values of the parameter g_{11} or g_{12} (whichever is nonvanishing) are determined by a combination of superconductivity and dephasing. Without superconductivity, $g_{11} = 1$, which results in a QH transition seen between the two quantized values of $G_{12} = 1$ to $G_{12} = 0$ with no intervening plateau. The introduction of superconductivity on a disordered chiral edge allows for Andreev scattering which gives rise to an intervening plateau. However, to obtain an intervening plateau that is stable at low temperatures one must account for dephasing through tunneling from the chiral edge into the disjointed chiral loops L_n (seen in Fig. 1). The nonvanishing conductance g_{11} or g_{12} (depending on whether $p > p_c$ or not) is determined by the transconductance $g_{\rm trans}$ across the incoherent chiral edge (coupled to an SC) that results from the tunneling into the loops L_n. To determine $g_{\rm trans}$ sufficiently close to the percolation point, where the loops L_n are expected to be larger than the finite-temperature and interaction-induced dephasing length $v\tau_\varphi$ (where v is the chiral edge velocity and τ_φ is the dephasing time), we assume the loop L_n to be a reservoir in equilibrium at voltage v_n (relative to the SC). Furthermore, we assume that the coupling between the loop L_n and the SC is weak enough to allow incoherent transfer of Cooper pairs through a resistance $R_n \sim v\{L\tau_\varphi[\Delta_s(x_n)]^2\}^{-1}$ between them. To understand the origin of the resistance R_n, we consider tunneling between the chiral loop and the SC which leads to a conductance $G_S \sim n_{\rm ch}G_N^2$ [22] where $n_{\rm ch}$ is the number of low-energy states (energy range of $\sim\tau_\varphi^{-1}$) in the chiral loop. The proximity gap $\Delta_s \propto G_N$ is proportional to the normal-state conductance G_N per channel. Given the voltages v_n and the voltage difference $V_{\rm in} - V_3$ between the incoming edge and the SC, the transconductance is given by [23]

$$g_{\rm trans} = \Lambda_{\rm in,out} + \sum_n \Lambda_{n,\rm out}\frac{v_n}{V_{\rm in} - V_3}, \quad (6)$$

where $\Lambda_{\rm in,out}$ and $\Lambda_{n,\rm out}$ are conductances obtained from the multiterminal Landauer-Büttiker formalism [24]. Specifically, the incoherent chiral edge may be thought of as a multiterminal system with leads at the *in* and *out* ends as well as each of the loops L_n. We can then define the response of the current in lead n to the voltage in lead m by

$$\Lambda_{mn} = \int_{-\infty}^{\infty} dE\left(-\frac{\partial f_T(E)}{\partial E}\right)\left[\left|t_{mn}^N(E)\right|^2 - \left|t_{mn}^A(E)\right|^2\right], \quad (7)$$

where $f_T(E) = 1/(e^{E/T}+1)$ is the Fermi distribution, $t_{mn}^N(E)$ and $t_{mn}^A(E)$ are the normal and Andreev scattering amplitudes at energy E, respectively, from the lead m into the lead n. Given Λ_{mn}, the voltages v_n, that appear in Eq. (6), can be determined recursively as one follows the loops down the chiral edge which are given by

$$\frac{v_n}{V_{\rm in} - V_3} = \frac{\Lambda_{{\rm in},n} + \sum_{m<n}\Lambda_{mn}\frac{v_m}{V_{\rm in}-V_3}}{R_n^{-1} + \Lambda_{n,\rm out} + \sum_{m>n}\Lambda_{nm}}. \quad (8)$$

These relations as well as Eq. (6) can be derived from the current conservation equation at each loop as detailed in the Supplemental Material [23].

The scattering amplitudes $t_{mn}^{N,A}$ are the components of 2×2 transmission (along the chiral edge) matrices acting in the particle-hole basis which is given by

$$\mathcal{T}_{mn}(E) = \begin{pmatrix} t_{mn}^N(E) & t_{mn}^{A*}(-E) \\ t_{mn}^A(E) & t_{mn}^{N*}(-E)\end{pmatrix}. \quad (9)$$

The inhomogeneity of the chemical potential and pairing potential along the loop is accounted by matching the incoming and outgoing edge modes in the SC region with spatially varying $\mu(x)$ and $\Delta(x)$, where (see the Supplemental Material [25] for the derivation)

$$\mathcal{T}_{mn}(E) = \zeta_{mn}\prod_{m<j<n} e^{i\tilde{v}_j^{-1/2}(\mu_j\tau_z + E\tau_0)\tilde{v}_j^{-1/2}\ell}, \quad (10)$$

with $\tilde{v}_j = v\tau_0 + \Delta_j\tau_x$ being the effective edge mode velocity at lattice site j and ℓ being the lattice constant. Here $\zeta_{mn} = \Omega_m\Omega_n\prod_{m<j<n}(1-\Omega_j^2)^{1/2}$ is a numerical factor that is related to the couplings $|\Omega_j| < 1$ of the chiral edge to the lead j ($\Omega_{\rm in} = \Omega_{\rm out} \equiv 1$).

From Eq. (10), we calculate the zero-bias net scattering probability Λ_{mn} [Eq. (7)] which is then used to compute the transconductance $g_{\rm trans}$ of a chiral edge [Eq. (6)], which is ultimately used to compute the two-terminal conductance [Eqs. (4) and (5)]. Figure 3 shows the calculated $g_{\rm trans}$ as a function of the electron trajectory length $L/\overline{\eta}$ where $\overline{\eta} = v k_{\rm so}/\overline{\Delta}_s$ is the mean value of the dimensionless p-wave superconducting coherence length with $k_{\rm so} \sim (50\ {\rm nm})^{-1}$. From Fig. 3, we can see that $g_{\rm trans}$ decays exponentially with L. The electron trajectory length L increases as the proportion $p \to p_c$ where the percolation threshold p_c corresponds to the magnetic field near the coercive field. Near p_c, L obeys the scaling relation [26],

$$L = L_0|p - p_c|^{-\nu d_h} = L_0|p - p_c|^{-(1+\nu)}, \quad (11)$$

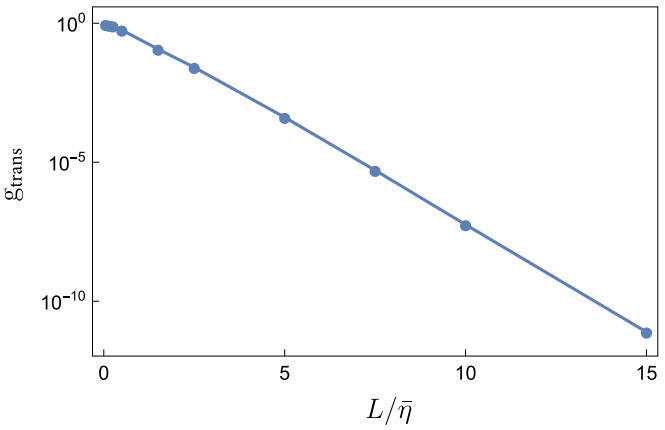

FIG. 3. Semilogarithmic plot of zero-energy effective transconductance $g_{\rm trans}$ vs electron trajectory length $L/\overline{\eta}$ where $\overline{\eta} = v/\overline{\Delta}$ is the average dimensionless p-wave superconducting coherence length. We consider spatially varying $\Delta(x)$ and $\mu(x)$ where the values of $\Delta(x) \in [0,0.1]$ and $\mu(x) \in [-0.01,0.01]$ are drawn from uniform distributions. Note that $g_{\rm trans}$ exponentially decays with L. For $p < p_c$, $g_{\rm trans} = g_{12} = g_{21}$ and $g_{11} = g_{22} = 0$, whereas for $p > p_c$, $g_{\rm trans} = g_{11} = g_{22}$ and $g_{12} = g_{21} = 0$. Parameters used are edge mode velocity $v = 1$, temperature $T = 0.01$, resistance $R(x) = 0.1/\{L[\Delta(x)]^2\}$, and coupling between the edge state and loop $\Omega(x) = 0.3$ for all x's.

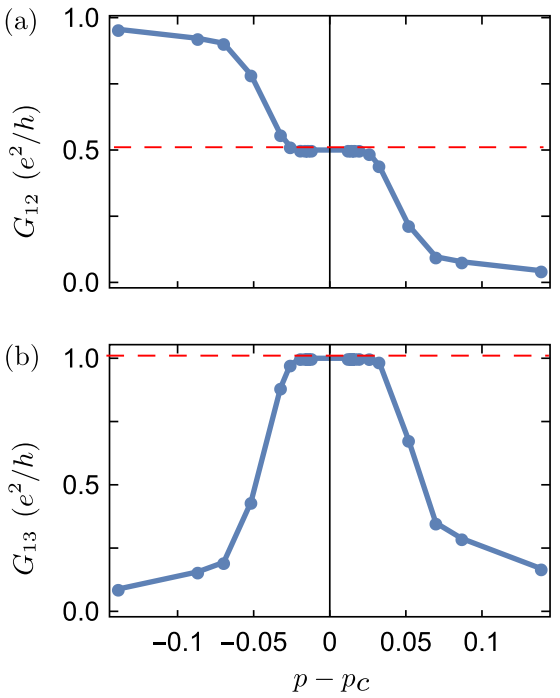

FIG. 4. Conductances (a) G_{12} and (b) G_{13} as a function of p near the percolation threshold p_c. G_{12} exhibits a half-integer quantized plateau at $p = p_c$, whereas G_{13} shows an integer quantized peak at $p = p_c$. The red dashed lines denote (a) $G = e^2/2h$ and (b) $G = e^2/h$. We set L_0 in Eq. (11) to be $\overline{\eta}/2000$ so that the conductance plateaus have a short width near p_c. The parameters used here are the same as those used in Fig. 3. The plateau width is stable at relatively low temperatures where the plateau width does not change in the low-temperature regime.

where for the 2D case considered here, the correlation length exponent ν is $\frac{4}{3}$ [27] and the fractal dimension of the hull d_h is $(1+\nu)/\nu$ [28]. Using Eqs. (6)–(11), we have $g_{\rm trans} \to 0$ as $p \to p_c$.

Next, we computed G_{12} and G_{13} using Eqs. (4) and (5), respectively, for a specific disorder realization. Figure 4 shows the numerically calculated G_{12} and G_{13} as functions of $p - p_c$ near the percolation threshold p_c. As seen from the plot, the conductance $G_{12} \simeq e^2/h$ for $p < p_c$ and $G_{12} \simeq 0$ for $p > p_c$ with an exponentially flat $e^2/2h$ plateau at p_c whereas the conductance $G_{13} \simeq 0$ for $p < p_c$ and $p > p_c$ with an e^2/h peak at p_c. Close to p_c, we can write G_{12} and G_{13} by using Eqs. (4)–(11) as

$$G_{12} \approx \begin{cases} \frac{e^2}{2h}(1 + e^{-2\alpha|p-p_c|^{-(1+\nu)}}) & \text{for } p = p_{c-} \\ \frac{e^2}{2h}(1 - e^{-2\alpha|p-p_c|^{-(1+\nu)}}) & \text{for } p = p_{c+}, \end{cases} \tag{12}$$

and

$$G_{13} \approx \begin{cases} \frac{e^2}{h}(1 - e^{-4\alpha|p-p_c|^{-(1+\nu)}}) & \text{for } p = p_{c-}, \\ \frac{e^2}{h}(1 - e^{-2\alpha|p-p_c|^{-(1+\nu)}}) & \text{for } p = p_{c+}, \end{cases} \tag{13}$$

where α is the inverse length scale for the exponential decay of $g_{\rm trans}$. At $p = p_c$, G_{12} and G_{13} are perfectly quantized at $e^2/2h$ and e^2/h, respectively, with exponentially flat plateaus. These plateaus, which originate from the disorder effect, resemble the experimental data [14] claimed to be the signatures of CMEMs. The width of the disorder-induced plateau decreases with decreasing pairing amplitude Δ as discussed in the Supplemental Material [29].

Our results, based on a classical percolation model for the QH transition, are valid at high temperatures where the chiral edge becomes effectively long enough to produce the plateaus in Fig. 4. This classical percolation picture is a reasonable description of the QH transition away from the critical point, at a relatively high temperature [15], or in the presence of dephasing arising from the interplay of interaction, disorder, and temperature [30]. Such dephasing requires the equilibration rate of quasiparticles in the loop being fast compared to tunneling as in our simple model of dephasing. The equilibration rate goes to zero as $T \to 0$. However, for appropriate interaction strengths and pairing potentials, the condition of strong dephasing can be satisfied to arbitrarily low temperatures leading to a weakly temperature-dependent plateau at low temperatures [31]. On the other hand, the plateau that arises from thermal fluctuations (without quasiparticle leakage between the chiral edge and the adjacent chiral loops) is strongly temperature dependent [31].

The $e^2/2h$ plateau shown in Fig. 4 would describe results not only in phases other than the $\mathcal{N} = 1$ TSC, but also in the $\mathcal{N} = 1$ phase for temperatures above the topological gap. At such high temperatures, $g_{\rm trans}$ would vanish because the edge quasiparticles could escape into the bulk by thermal excitations which makes it difficult to ascribe the conductance plateau to the topological properties of the TSC. Additionally, it has been proposed that, in the limit of strong disorder, the gapped $\mathcal{N} = 1$ TSC may be replaced by a gapless Majorana metal phase even at zero temperature [32], which may also produce an $e^2/2h$ plateau.

Although our results do not contradict the theoretical existence of the $\mathcal{N} = 1$ TSC phase (which is likely although not inevitable) in the vicinity of the QAH transition, the nearly quantized $e^2/2h$ conductance plateau observed in the recent experiment [14] cannot serve as an experimental evidence for the $\mathcal{N} = 1$ TSC as it is likely to arise outside the TSC phase as well. In principle, observing the stabilization of the plateau to a more perfectly quantized plateau as the temperature is lowered together with either a hard superconducting gap from the electrical conductance measurement (which is unlikely for a disordered system) or a thermal transport gap would be the signatures of an $\mathcal{N} = 1$ TSC. Another smoking-gun signature is the half-quantized thermal conductivity $K_H = (\pi k_B)^2 T/6h$ [33] which would rule out the classical percolation-based model and the Majorana metal phase as they would have a large nonuniversal longitudinal thermal conductance.

Note added. Upon completion of our Rapid Communication, we became aware of a recent paper [34] related to our work.

We thank K. T. Law for valuable discussions that drew our attention to Ref. [14], which motivated this Rapid Communication. J.D.S. acknowledges stimulating discussions with S.-C. Zhang that motivated the discussion of the low-temperature limit. We also thank Y. Alavirad, C.-K. Chiu, and Q.-L. He for helpful discussions. This Rapid Communication was supported by JQI-NSF-PFC, Sloan Research Fellowship and Grant No. NSF-DMR-1555135 (CAREER). Y.H. is grateful to the China Scholarship Council for financial support. We acknowledge the University of Maryland supercomputing resources [35] made available in conducting the research reported in this Rapid Communication.

[1] C. Nayak, S. H. Simon, A. Stern, M. Freedman, and S. Das Sarma, Rev. Mod. Phys. **80**, 1083 (2008).
[2] N. Read and D. Green, Phys. Rev. B **61**, 10267 (2000).
[3] D. A. Ivanov, Phys. Rev. Lett. **86**, 268 (2001).
[4] X.-L. Qi, T. L. Hughes, and S.-C. Zhang, Phys. Rev. B **82**, 184516 (2010).
[5] S. B. Chung, X.-L. Qi, J. Maciejko, and S.-C. Zhang, Phys. Rev. B **83**, 100512 (2011).
[6] J. Wang, Q. Zhou, B. Lian, and S.-C. Zhang, Phys. Rev. B **92**, 064520 (2015).
[7] X.-L. Qi, Y.-S. Wu, and S.-C. Zhang, Phys. Rev. B **74**, 085308 (2006).
[8] C.-X. Liu, X.-L. Qi, X. Dai, Z. Fang, and S.-C. Zhang, Phys. Rev. Lett. **101**, 146802 (2008).
[9] C.-X. Liu, S.-C. Zhang, and X.-L. Qi, Annu. Rev. Condens. Matter Phys. **7**, 301 (2016).
[10] R. Yu, W. Zhang, H.-J. Zhang, S.-C. Zhang, X. Dai, and Z. Fang, Science **329**, 61 (2010).
[11] C.-Z. Chang, J. Zhang, X. Feng, J. Shen, Z. Zhang, M. Guo, K. Li, Y. Ou, P. Wei, L.-L. Wang *et al.*, Science **340**, 167 (2013).
[12] J. Wang, B. Lian, and S.-C. Zhang, Phys. Rev. B **89**, 085106 (2014).
[13] C.-Z. Chang, W. Zhao, J. Li, J. K. Jain, C. Liu, J. S. Moodera, and M. H. W. Chan, Phys. Rev. Lett. **117**, 126802 (2016).
[14] Q. L. He, L. Pan, A. L. Stern, E. C. Burks, X. Che, G. Yin, J. Wang, B. Lian, Q. Zhou, E. S. Choi, K. Murata, X. Kou, Z. Chen, T. Nie, Q. Shao, Y. Fan, S.-C. Zhang, K. Liu, J. Xia, and K. L. Wang, Science **357**, 294 (2017).
[15] J. Chalker and P. Coddington, J. Phys. C: Solid State Phys. **21**, 2665 (1988).
[16] C.-Z. Chen, J. J. He, D.-H. Xu, and K. T. Law, Phys. Rev. B **96**, 041118 (2017).
[17] M. Z. Hasan and C. L. Kane, Rev. Mod. Phys. **82**, 3045 (2010).
[18] See Supplemental Material at http://link.aps.org/supplemental/10.1103/PhysRevB.97.100501 for the derivation of the effective p-wave pairing potential Δ from the minimal QAH two-band model in Sec. I.
[19] M. P. Anantram and S. Datta, Phys. Rev. B **53**, 16390 (1996).
[20] O. Entin-Wohlman, Y. Imry, and A. Aharony, Phys. Rev. B **78**, 224510 (2008).
[21] Y. Takane and H. Ebisawa, J. Phys. Soc. Jpn. **61**, 1685 (1992).
[22] C. W. J. Beenakker, Phys. Rev. B **46**, 12841 (1992).
[23] See Supplemental Material at http://link.aps.org/supplemental/10.1103/PhysRevB.97.100501 for the dephasing model of the chiral edge states in Sec. II.
[24] S. Datta, *Electronic Transport in Mesoscopic Systems* (Cambridge University Press, Cambridge, U.K., 1997).
[25] See Supplemental Material at http://link.aps.org/supplemental/10.1103/PhysRevB.97.100501 for a detailed derivation of the scattering matrix in Sec. III.
[26] M. B. Isichenko, Rev. Mod. Phys. **64**, 961 (1992).
[27] B. Nienhuis, Phys. Rev. Lett. **49**, 1062 (1982).
[28] B. Sapoval, M. Rosso, and J.-F. Gouyet, J. Phys. Lett. **46**, 149 (1985).
[29] See Supplemental Material at http://link.aps.org/supplemental/10.1103/PhysRevB.97.100501 for the dependence of the plateau width on the pairing potential in Sec. IV.
[30] A. Kapitulnik, N. Mason, S. A. Kivelson, and S. Chakravarty, Phys. Rev. B **63**, 125322 (2001).
[31] See Supplemental Material at http://link.aps.org/supplemental/10.1103/PhysRevB.97.100501 for the dephasing model via random thermal fluctuations in Sec. V.
[32] T. Senthil and M. P. A. Fisher, Phys. Rev. B **61**, 9690 (2000).
[33] C. L. Kane and M. P. A. Fisher, Phys. Rev. B **55**, 15832 (1997).
[34] W. Ji and X.-G. Wen, Phys. Rev. Lett. **120**, 107002 (2018).
[35] http://www.it.umd.edu/hpcc.